Information content of the low-energy electric dipole strength: Correlation analysis

P.-G. Reinhard and W. Nazarewicz

Phys. Rev. C **87**, 014324 — Published 18 January 2013

DOI: 10.1103/PhysRevC.87.014324

Information content of the low-energy electric dipole strength: correlation analysis

P.–G. Reinhard[1] and W. Nazarewicz[2, 3, 4]

[1] *Institut für Theoretische Physik II, Universität Erlangen-Nürnberg, Staudtstrasse 7, D-91058 Erlangen, Germany*
[2] *Department of Physics & Astronomy, University of Tennessee, Knoxville, Tennessee 37996, USA*
[3] *Physics Division, Oak Ridge National Laboratory, Oak Ridge, Tennessee 37831, USA*
[4] *Institute of Theoretical Physics, University of Warsaw, ul. Hoża 69, 00-681 Warsaw, Poland*

Background: Recent experiments on the electric dipole (E1) polarizability in heavy nuclei have stimulated theoretical interest in the low-energy electric dipole strength, both isovector and isoscalar.

Purpose: We study the information content carried by the electric dipole strength with respect to isovector and isoscalar indicators characterizing bulk nuclear matter and finite nuclei. To separate isoscalar and isovector modes, and low-energy strength and giant resonances, we analyze the E1 strength as a function of excitation energy E and momentum transfer q.

Methods: We use the self-consistent nuclear density functional theory with Skyrme energy density functionals, augmented by the random phase approximation, to compute the E1 strength, and covariance analysis to assess correlations between observables. Calculations are performed for spherical, doubly-magic nuclei ^{208}Pb and ^{132}Sn.

Results: We demonstrate that E1 transition densities in the low-energy region below the giant dipole resonance exhibit appreciable state dependence and multi-nodal structures, which are fingerprints of weak collectivity. The correlation between the accumulated low-energy strength and symmetry energy is weak, and dramatically depends on the energy cutoff assumed. On the other hand, a strong correlation is predicted between isovector indicators and the accumulated isovector strength at E around 20 MeV and momentum transfer $q \sim 0.65\,\mathrm{fm}^{-1}$.

Conclusions: Momentum- and coordinate-space pattern of the low-energy dipole modes indicate a strong fragmentation into individual particle-hole excitations. The global measure of low-energy dipole strength poorly correlates with the nuclear symmetry energy and other isovector characteristics. Consequently, our results do not support the suggestion that there exists a collective "pygmy dipole resonance," which is a strong indicator of nuclear isovector properties. By considering nonzero values of momentum transfer, one can isolate individual excitations and nicely separate low-energy excitations from the $T = 1$ and $T = 0$ giant collective modes. That is, measurements at $q > 0$ may serve as a tool to correlate the E1 strength with certain bulk observables, such as incompressibility or symmetry energy.

PACS numbers: 21.10.Pc, 21.60.Jz, 21.65.Mn 24.30.Cz

I. INTRODUCTION

The electric dipole response of the atomic nucleus carries fundamental information on bulk nuclear properties and shell structure [1–9] and it also plays an important role in nuclear reactions involving photo-nuclear processes. In particular, E1 strength impacts photoabsorption and radiative particle-capture processes occurring in stars during the cosmic nucleosynthesis [10] and the transmutation of radioactive nuclear waste [11].

The significance of the E1 strength, especially in the context of neutron-rich nuclei, has led to appreciable experimental progress in this area [12–19]. Much excitement has been brought by a suggestion that the low-energy E1 strength, dubbed "Pygmy Dipole Resonance" (PDR) [20, 21], is collective in nature, and can be understood as a motion of skin neutrons against the proton-neutron core.

The current theoretical situation regarding the collectivity of the low-energy E1 strength is fairly confusing. While some papers advocate the existence of a collective PDR mode [16, 18, 22–25], having strength that is correlated with the nuclear symmetry energy [16, 22, 23], the collectivity of the low-energy E1 transitions, and their relevance to isovector nuclear matter properties (NMP), have been questioned by several other studies [26–31]. A recent study of a flow pattern in low-energy E1 modes confirms these doubts [32].

In particular, the covariance analysis of Ref. [26] has suggested the lack of correlation between PDR strength and nuclear isovector properties, such as neutron-skin thickness r_{skin} and symmetry energy. One reason for this was attributed to the local single-particle structure around the Fermi level (i.e., shell effects), which vary rapidly with global nuclear matter characteristics. On the other hand, the dipole polarizability α_{D} – a global measure of the E1 strength – seems to be an excellent isovector indicator [19, 26, 33, 34]. Similar conclusions have been reached in Ref. [28], which concluded that the current data on the low-energy strength, and theoretical predictions, are both too uncertain for a quantitative analysis.

The aim of this work is to clarify the situation by means of the stringent correlation analysis based on methods of data analysis using least-squares optimization. We will consider, in particular, the correlations between various nuclear observables (including NMP and properties of finite nuclei) and E1 strength. Our paper is organized as follows. Section II describes our nuclear EDF+RPA approach and motivates the choice of EDFs used. The definitions pertaining to E1 form fac-

tors, strength functions, and resulting E1 sum rules are discussed in Sec. III. The dependence of the low-energy E1 strength on selected nuclear matter properties is studied in Sec. V. The results for transition densities are presented in Sec. IV, and Sec. VI contains the correlation analysis. While most calculations in this study were done for ^{208}Pb, Sec. VII contains illustrative examples for ^{132}Sn that demonstrate that our findings are general. Finally, Sec. VIII contains conclusions of the work.

II. MODEL

The present investigation is based on the self-consistent nuclear density functional theory in the Skyrme-Hartree-Fock (SHF) variant [35, 36]. The form of the SHF energy density functional (EDF) is derived from rather general arguments of a low-momentum expansion [37, 38]. However, since the coupling constants of EDF cannot be determined precisely from underlying nuclear forces, they are usually adjusted to selected nuclear data [35, 39, 40]. We use here two recent EDF parameterizations which try to embrace a large collection of various nuclear data [39, 41]. The survey [39] selected a pool of spherical nuclei which have been checked to be well described by a mean-field model [42]. The resulting parameterization SV-min was optimized by means of a least-squares procedure. Its (parabolic) least-squares landscape $\chi^2 = \chi^2(\mathbf{p})$, where $\mathbf{p}$ stands for the multitude of SHF parameters, carries important information on the uncertainties, in particular on model features that are weakly determined by the optimization process. This can be exploited by applying the standard covariance analysis as was done, e.g., in Refs. [26, 43]. To estimate the uncertainty related to the choice of fit observables, we alternatively look at the parameterization UNEDF0 [41], which covers a much larger set of ground state data, also including many deformed nuclei.

It is found that many aspects of EDF can be characterized by relatively few NMP, such as incompressibility K, isoscalar effective mass m^*/m, symmetry energy $a_{\rm sym}$, and Thomas-Reiche-Kuhn (TRK) sum rule enhancement κ (related to the isovector effective mass). By providing a set of parameterizations for which these NMP are systematically varied [39], one can track explicitly the influence of the NMP on various nuclear properties. Base point of this set is the EDF called SV-bas, for which four NMP had been fixed: $K = 234$ MeV, $m^*/m = 0.9$, $a_{\rm sym} = 30$ MeV, and $\kappa = 0.4$ (chosen such that the giant dipole resonance (GDR) in ^{208}Pb is described correctly). Starting from SV-bas, four sets of parameterizations were produced [39] by systematic variation of each one of the four NMP. It is to be noted that SV-bas and its systematically varied sister parameterizations are adjusted with additional constraints on NMP. SV-min, on the other hand, is fitted only to data from finite nuclei and thus covers all uncertainty on NMP as left open by nuclear ground state data, a feature which make it ideally suited for our covariance analysis.

The focus of our survey is on properties of nuclear excitations in the electric dipole channel. To compute the E1 strength function, we employ the random phase approximation (RPA), using the same EDF as for the ground state to guarantee the full self-consistency. The details of RPA calculations follow Ref. [44, 45].

III. STRENGTH FUNCTIONS

In the following, we discuss various aspects of the electric dipole strength, both isoscalar ($T = 0$) and isovector ($T = 1$). Detailed information on the strength is contained in the dipole transition form factor:

$$F_\nu^{(T)}(q) = \langle \Psi_\nu | \sum_{\alpha=1}^{A} j_1(qr_\alpha) Y_{10}(\Omega_\alpha) \hat{\Pi}_T | \Psi_0 \rangle \qquad (1)$$

where α runs over all nucleons, Ψ_ν is the wave function of the ν-th RPA excitation, Ψ_0 the ground state wave function, q is momentum transfer, T is the isospin quantum number, and $\hat{\Pi}_T$ stands for the isospin projector:

$$\hat{\Pi}_0 = \hat{\Pi}_{\rm prot} + \hat{\Pi}_{\rm neut} \ , \ \hat{\Pi}_1 = \frac{N}{A}\hat{\Pi}_{\rm prot} - \frac{Z}{A}\hat{\Pi}_{\rm neut}. \qquad (2)$$

(For spherical nuclei, such as ^{208}Pb and ^{132}Sn considered in this work, it is sufficient to consider the single mode with the magnetic quantum number $\mu = 0$.) The q-dependence carries the pattern of an excitation mode. A complementing coordinate-space view is provided by radial transition density, which is the Fourier transform of $F_\nu^{(T)}(q)$:

$$\rho_\nu^{(T)}(r) = 4\pi \int_0^\infty dq\, q^2\, j_1(qr)\, F_\nu^{(T)}(q). \qquad (3)$$

Since the RPA excitation spectrum of a heavy nucleus such as ^{208}Pb is fairly dense, it is more convenient to consider the energy distribution of form factor strength:

$$S_F^{(T)}(q,E) = \frac{1}{q^2} \sum_\nu |F_\nu^{(T)}(q)|^2 \mathcal{G}_\Gamma(E - E_\nu), \qquad (4)$$

where E_ν is the RPA excitation energy of state ν and $\mathcal{G}_\Gamma(E - E_N)$ is a Gaussian folding function having energy-dependent width $\Gamma(E_\nu) = \max[0.2\,\text{MeV}, (E_\nu - 8\,\text{MeV})/6\,\text{MeV}]$ – to simulate nuclear damping effects, which increase with energy. We note small Γ (and improved resolution) in the low energy region, which is the very focus of this work.

The factor q^{-2} in Eq. (4) is introduced to cancel the leading q^2-dependence of $F_\nu^{(T)}(q)$ at small momentum transfer. Indeed, at $q \to 0$, the isovector strength $S_F^{(1)}(q,E)$ is proportional to that of the familiar dipole operator $\hat{D} = rY_{10}\hat{\Pi}_1$, which we denote by $S_D(E)$. The next-order term in q leads to the "compressional dipole"

operator $\hat{D}_c^{(T)} = (r^3 - \frac{5}{3}\langle r^2\rangle r)Y_{10}\hat{\Pi}_T$, the leading observable in the isoscalar channel [46–50], and the corresponding strength is denoted by $S_{D_c}^{(T)}(E)$. For energy cuts at finite q, we shall consider the general dipole operator $\hat{F} = j_1(qr)Y_{10}\hat{\Pi}_T$ as in Eq. (1).

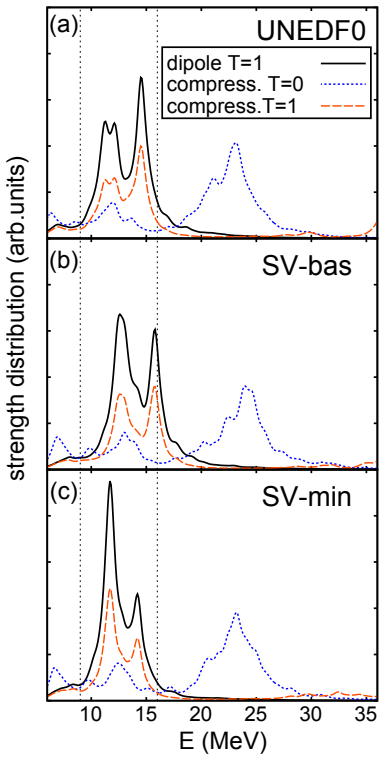

FIG. 1. (Color online) Isoscalar and isovector E1 strength S_D (solid line), $S_{D_c}^{(0)}$ (dotted line), and $S_{D_c}^{(1)}$ (dashed line) in ^{208}Pb predicted with (a) UNEDF0, (b) SV-bas, and (c) SV-min EDFs. The region of GDR is marked by vertical dotted lines; these limits are somewhat arbitrary as the GDR strength does not show clear energy bounds.

To assess the importance of the low-energy E1 strength, we introduce the accumulated strength:

$$A_n^{\mathcal{O}}(E) = \int_0^E dE'\, E'^n\, S_{\mathcal{O}}(E'), \tag{5}$$

where $\mathcal{O}$ can mean either the mere dipole D, compressional dipole D_c, or general dipole F at a given value of q. In Eq. (5), we use a constant folding width $\Gamma = 0.5$ MeV in $S_{\mathcal{O}}$. For the dipole operator, the inverse-energy-weighted sum rule $A_{-1}^D(\infty)$ is related to the electric dipole polarizability [5]

$$\alpha_{\rm D} = 2 \sum_{\nu\in{\rm RPA}} (|\langle\Psi_\nu|\hat{D}|\Psi_0\rangle|^2/E_\nu), \tag{6}$$

while the energy-weighted sum rule $A_1^D(\infty)$ is the TRK sum rule.

Figure 1 shows E1 strength $S_D(E)$ and $S_{D_c}^{(T)}(E)$ in ^{208}Pb predicted with UNEDF0, SV-bas, and SV-min EDFs. The isovector dipole strength S_D is concentrated in the GDR region of 12-16 MeV. The systematic shift of the GDR strength between EDFs reflects the change in TRK sum rule enhancement (κ=0.4 for SV-bas, 0.25 for UNEDF0, and 0.08 for SV-min) [39]. The isovector compressional strength $S_{D_c}^{(1)}$ roughly follows S_D. It does also contain a high energy branch above 30 MeV which, however, is not of interest in the context of this study. The isoscalar compressional strength is fairly broad, with a low-energy component at 5-18 MeV and a high-energy concentration at 20-30 MeV [8].

Using the standard representation of E1 strength as shown in Fig. 1, it is difficult to separate the low-energy strength from the tails of giant resonance modes. A better separation can be obtained by considering nonzero values of q, i.e., by analyzing the full distribution $S_F^{(T)}(q,E)$. Figure 2 shows the structure of the E1 strength (4) – together with individual proton and neutron strength distributions – for SV-bas in the (E,q) plane. As expected, the isoscalar channel shown in

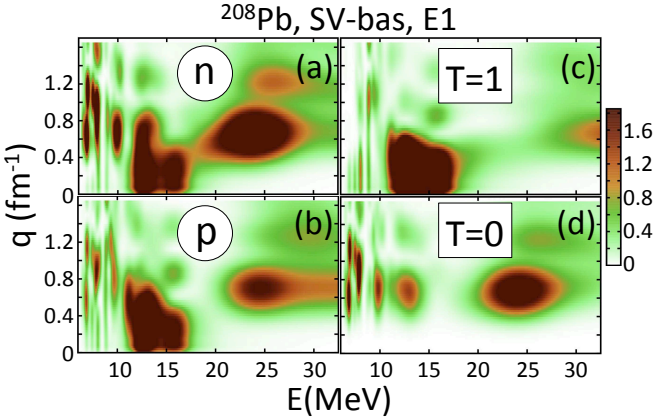

FIG. 2. (Color online) E1 strength (4) for ^{208}Pb computed with SV-bas as a function of E and q. (a) Neutron strength; (b) proton strength; (c) $T = 1$ strength (scaled by 2); and (d) $T = 0$ strength (scaled by 0.25). Since S_F rapidly decreases with q, rather than the actual strength (4) we show the q-scaled strength $\tilde{S}_F^{(T)}(q,E) = S_F^{(T)}(q,E)(1+a_q q^2)^2$ with $a_q = 9\,{\rm fm}^2$.

Fig. 2(d) has no strength at $q \to 0$, as the spurious isoscalar collective center-of-mass E1 mode is removed in our calculations. The large isoscalar strength appears at somewhat larger momentum transfer around $q = 0.65{\rm fm}^1$. Therein, one can clearly see the two branches of the isoscalar dipole compressional mode at 6-13 MeV and 24 MeV. The GDR centered around 13 MeV dominates the $T = 1$ strength at low values of q. It seems that the group of excitations between 6 and 11 MeV has predominantly isoscalar compressional character. They seem to be higher-q extensions of some low-energy isovector dipole strength (often referred to as PDR strength). These low-energy dipole transitions can thus be considered as shadows of the low-energy dipole compressional modes. The neutron and proton E1 strengths displayed

in Figs. 2(a) and (b), respectively, show that the states having large transition form factors are *all* mixed proton and neutron excitations. While the neutrons carry more strength generally, pure neutron modes do not appear.

The upper branch of the compressional mode around 22–26 MeV shown in Fig. 2 is not so interesting for our study. Therefore, in the following, we will restrict the energy range. Figure 3 illustrates the low-energy pattern of the E1 strength for three EDFs of Fig. 1. It is encouraging to see that the general behavior of E1 strength is EDF-independent, so the detailed discussion of RPA modes will be based on SV-bas calculations. In the energy range below 10 MeV, only a handful of modes can be seen. Actually, we find more RPA states (e.g., 20 modes between 6 and 10 MeV) in that range, but only a third of them are visible in E1 excitation. These strong-E1, low-E modes have a fairly diverse character. The lowest states below 7.5 MeV are predominantly isoscalar in character, having some contribution to the $T = 1$ channel. The mode at 8 MeV has a mixed character (isovector at low q-values and isoscalar at higher q), while the mode at 9 MeV is predominantly an isovector excitation. The states around 10 MeV are again dominated by $T = 0$. Their $T = 1$ component is weak, and it is mainly concentrated at larger q, i.e., these states do not carry significant dipole ($q = 0$) strength.

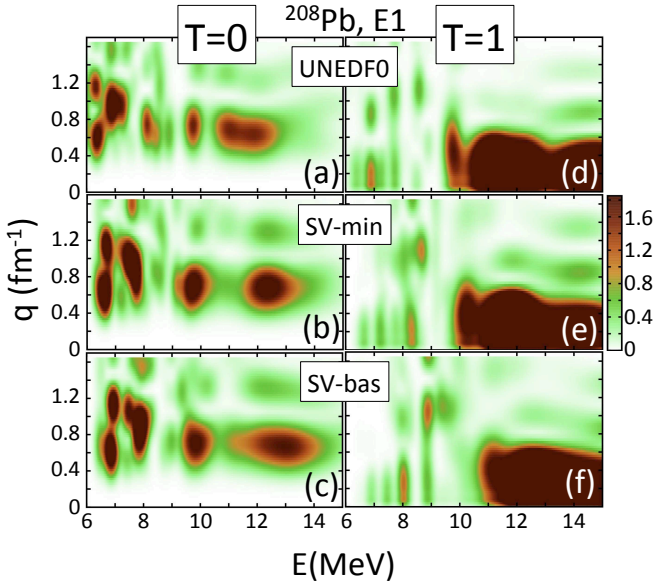

FIG. 3. (Color online) Similar as in Fig. 2 for $T = 0$ (left) and $T = 1$ (right) E1 strength computed with (a) UNEDF0, (b) SV-min, and (c) SV-bas EDFs.

IV. TRANSITION DENSITIES

The interesting question is to what extent the lowest E1 modes can be considered as collective, as discussed (or assumed) in some studies. To this end, it is instructive to study this point in the coordinate-space in terms of the transition density $\rho_\nu^{(T)}$ of Eq. (3). In order to present results as a function of E, we performed a Gaussian folding as in Eq. (4). Figure 4 depicts the general behavior of E1 transition density in ^{208}Pb as a function of E and r. At $E < 12$ MeV, $\rho^{(T)}$ varies rapidly with E, exhibiting a complex multi-nodal behavior in both isospin channels (cf. discussion in Refs. [34, 51]). The strong state dependence, together with the lack of a common pattern across the various nearly-lying states, both suggest a weak collectivity. A different situation is encountered in the GDR region. Although the energy band of 12-17 MeV covers a large number of RPA states, the $T = 1$ transition density has the same pattern of a pronounced surface bump in the whole GDR region. Note that we have plotted here the transition densities with an energy-dependent folding width to simulate a realistic broadening. However, we have checked that a very similar picture emerges at a higher resolution (i.e., using a small folding width of 0.2 MeV). A similar pattern, indicative of collectivity, is seen for the $T = 0$ compressional mode at 22-28 MeV. Such coherent behavior is characteristic of a collective mode.

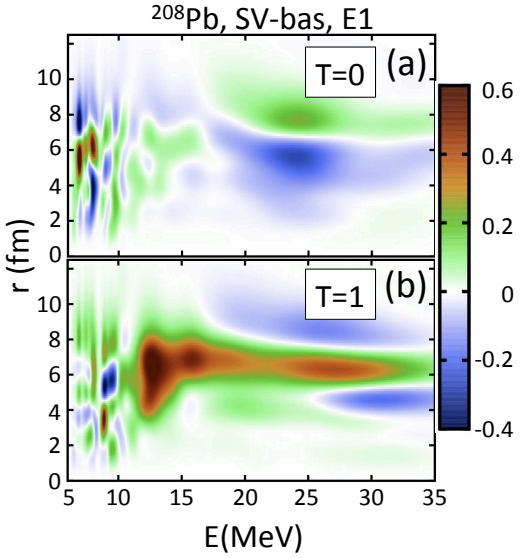

FIG. 4. (Color online) Energy-averaged E1 transition density in ^{208}Pb calculated with SV-bas as a function of E and r for $T = 0$ (top) and $T = 1$ (bottom).

V. LOW-ENERGY ELECTRIC DIPOLE STRENGTH

Although transition density and form factor reveal a world of local details, it is desirable to quantify their information content in terms of a few integrated quantities. One such quantity is the accumulated low-energy

E1 strength,

$$B(E1;E_{\max}) = \sum_{\nu\in\mathrm{RPA},E_\nu<E_{\max}} B(E1,\nu), \qquad (7)$$

which is proportional to the accumulated strength $A_0^D(E_{\max})$. This observable is somewhat ambiguous as it depends on an assumed cutoff energy $E_{\max}$. Figure 5 shows the predicted $B(E1;E_{\max})$ in ^{208}Pb as a function of two isoscalar (incompressibility K and isoscalar effective mass m^*/m) and two isovector (symmetry energy $a_{\rm sym}$ and TRK sum rule enhancement κ) NMP indicators [26]. The calculations were carried out with four sets of EDF parameterizations around SV-bas [39] by systematically varying the NMP of interest. We used the value $E_{\max}$=10 MeV that corresponds to the beginning of the GDR region in SV-bas, see Fig. 3.

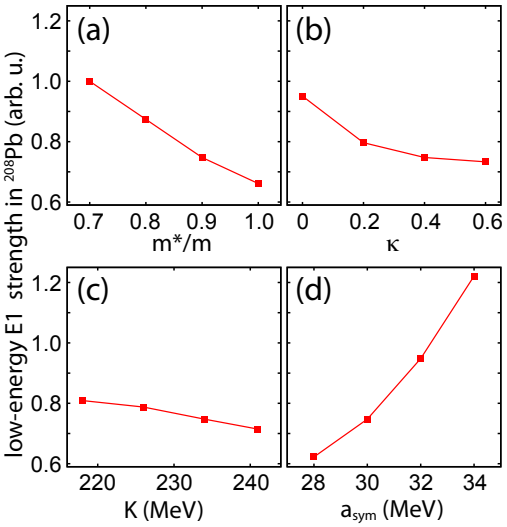

FIG. 5. (Color online) Dependence of the low-energy E1 strength (7) in ^{208}Pb on selected NMP: (a) m^*/m; (b) κ; (c) K; and (d) $a_{\rm sym}$. Calculations were carried out with SV-bas family of EDFs. The cutoff energy is $E_{\max}$=10 MeV.

When considering each variation independently, one can see a monotonic trend in each case. But does it mean that a well-defined correlation exists between the low-energy E1 strength and the bulk properties considered? Clearly, the answer to this question cannot be given based on Fig. 5 alone, as $B(E1;E_{\max})$ seems to depend on several NMP, both isoscalar and isovector in character, and the plot says nothing about the possible coupling between them as an underlying EDF parametrization is systematically varied. Second, if a parametrization is too constrained in a given interaction channel, *all* variations probing this channel are correlated by construction. (An example of such a situation was given in Ref. [26] in the context of a relativistic mean field model RMF-δ-t, too constrained in the isovector channel to be used in a meaningful correlation analysis.) Although the explicit tracking with respect to single NMP, as done in Fig. 5, can be very useful to uncover hidden dependencies between observables, it does not explore all conceivable variations and is thus insufficient to quantify true correlations. A more exhaustive method will be discussed in the next section.

VI. CORRELATIONS

Thus far we have analyzed the structure of dipole modes in terms of transition form factor and transition density. These structures do not show convincing signatures of collectivity in the low-energy region below GDR. As a more global measure, we inspected the integrated low-energy dipole strength, which indeed displays some complex dependence on NMP. For a more exhaustive (and quantitative) analysis, we will now exploit the stringent method of covariance analysis and scrutinize the correlations between integrated dipole observables and collective bulk properties (NMP, dipole polarizability, and neutron skin).

As already mentioned in section II, the empirical adjustment of EDF parameters produces a nearly-parabolic χ^2 landscape near the minimum, i.e., $\chi^2(\mathbf{p}) \approx \chi^2_0 + \sum_{ij} p_i p_j \partial^2_{p_i p_j} \chi^2$. The vicinity of the minimum in the $\mathbf{p}$-space, for which $\chi^2(\mathbf{p}) = \chi^2_0 + 1$, is considered as the space of acceptable parameter variations (1σ region). Observables are also functions of the EDF parameters: $A = A(\mathbf{p})$. A correlation between observables A and B within a given model can then be assessed by means of the correlation coefficient

$$C_{AB} = \frac{\overline{|\Delta A\,\Delta B|}}{\sqrt{\overline{\Delta A^2}\;\overline{\Delta B^2}}}, \qquad (8)$$

where the overline means an average over the space of acceptable parameters [24, 26, 43]. Such correlation analysis had been proven useful in previous surveys. For example, it was concluded that the electric dipole polarizability is a good isovector indicator that strongly correlates with the neutron radius of ^{208}Pb [24, 26].

The correlation between E1 strengths in ^{208}Pb and basic nuclear matter properties $(K, m^*/m, a_{\rm sym}, \kappa)$ is discussed in Figs. 6-8 as a function of E. Figure 6 illustrates the correlation with the accumulated dipole strength $A_n^D(E)$ (5). The case of $n = -1$ is shown in Fig. 6(a). As noted earlier, $A_{-1}^D(E)$ is the accumulator for the dipole polarizability $\alpha_{\rm D}$. It is interesting to see how the sensitivity to $a_{\rm sym}$ (and insensitivity to other NMP) develops at high energies. At GDR energies and below, however, the correlations vary dramatically. The changes are particularly rapid around the lower end of the GDR region (9-10 MeV), which is often used as a cutoff energy $E_{\max}$ to determine the low-energy E1 strength (7). It is apparent that even small changes in $E_{\max}$ may change correlations. This result casts serious doubts on standard (cutoff-dependent) definitions of the pygmy strength.

The corollary of the emerging specific sensitivity is seen in Fig. 6(b), which illustrates the case of $n = 1$. At large

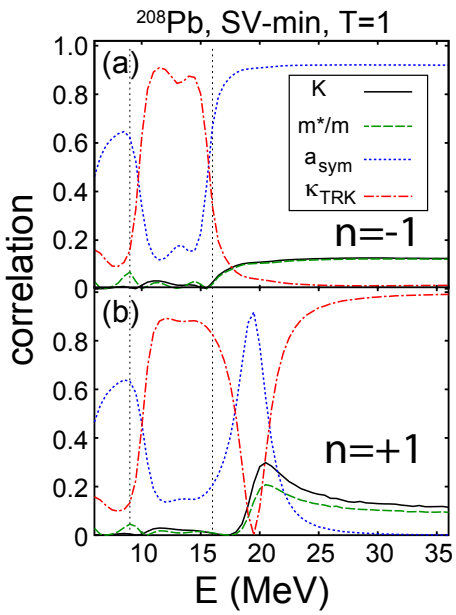

FIG. 6. (Color online) Correlation between the energy-weighted accumulated strength $A_n^D(E)$ (5) in ^{208}Pb and selected NMP (incompressibility K, isoscalar effective mass m^*/m, symmetry energy $a_{\rm sym}$, and TRK sum rule enhancement κ) as a function of E obtained with SV-min. Top: $n = -1$; bottom: $n = 1$. The GDR region is marked by vertical dotted lines.

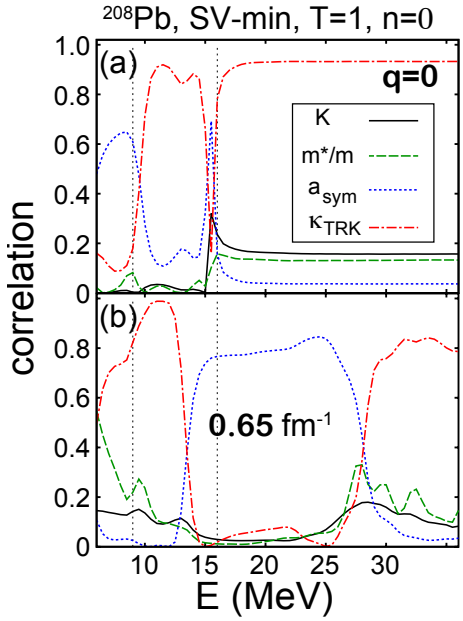

FIG. 7. (Color online) Similar to Fig. 6 but for the accumulated dipole strength $A_0^D(E)$ for two values of momentum transfer: (a) $q = 0$ and (b) $q = 0.65\,\mathrm{fm}^{-1}$.

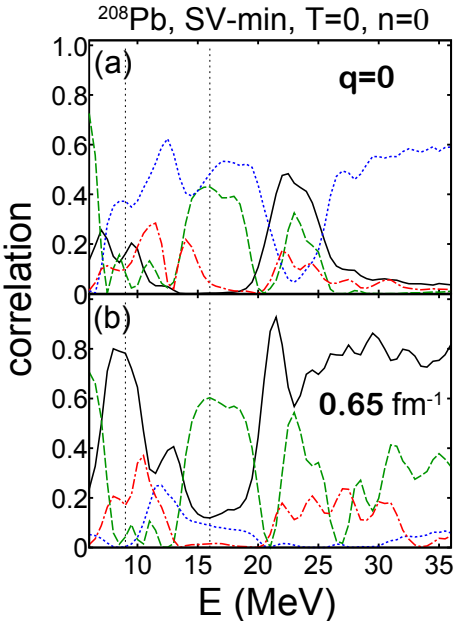

FIG. 8. (Color online) Similar as in Fig. 7 but for the $T = 0$ compressional dipole E1 strength.

energies, the accumulated dipole strength $A_1^D(E)$ develops into an unambiguous measure of κ. As expected, K and m^*/m never correlate with $A_{\pm1}^D(E)$, regardless of the energy region. This is to be expected as these NMP are isoscalar indicators [26].

The summed dipole strength $A_0^D(E)$ is often used as a measure of the pygmy mode. We show in Fig. 7 how it correlates with NMP. At zero momentum transfer, Fig. 7(a), the correlation pattern strongly resembles that of Fig. 6(b), including strong correlation with κ at high energies. The three cases displayed in Figs. 6 and 7(a) have certain common features. Namely, they all show (i) rapid changes near the lower and the upper end of the GDR region; (ii) strong correlation with κ in the GDR region; and (iii) medium correlation with $a_{\rm sym}$ around $E = 7\,\mathrm{MeV}$.

A stronger handle on $a_{\rm sym}$ is provided by the summed dipole strength $A_0^D(E)$ at nonzero momentum transfer. Figure 7(b) illustrates the case of integrated form factor strength at $q = 0.65\,\mathrm{fm}^{-1}$. A particularly large correlation with $a_{\rm sym}$ is predicted in a wide energy range above the GDR region and below 25 MeV. A strong correlation with κ in the GDR region still holds at this value of q.

The complementing $n = 0$ isoscalar strengths are shown in Fig. 8(a). At low values of q, the summed compressional dipole strength $A_0^{D_c}(E)$ contains little information on NMP. The sensitivity to $a_{\rm sym}$ at the low-E region, suggested in [34], is minor. Figure 8(b) demonstrates that some sensitivity to K appears at $q = 0.65\,\mathrm{fm}^{-1}$, especially at low energies below the GDR region and in the high energy region above 20 MeV.

We now turn to a correlation between isovector form factor strength $A_0^F(E)$ and the four strong isovector indicators: the slope of symmetry energy $a'_{\rm sym}$ at the saturation density, slope of the neutron EoS $E_{\rm neut}/N$ at neutron density $0.08\,\mathrm{fm}^3$, E1 polarizability $\alpha_{\rm D}$, and neutron-

skin thickness $r_{\rm skin}$ in ^{208}Pb. Recall that these four observables are highly correlated with each other and with $a_{\rm sym}$ [26]. Consequently, all four correlations displayed in Fig. 9 are practically identical, and also agree with the results for $a_{\rm sym}$ shown in Fig. 7: the summed isovector E1 strength ($n = 0$) above the GDR at the intermediate values of momentum transfer around $q = 0.65\,{\rm fm}^{-1}$ is an excellent isovector indicator. As illustrated in Fig. 9(c), however, this correlation deteriorates at higher values of q.

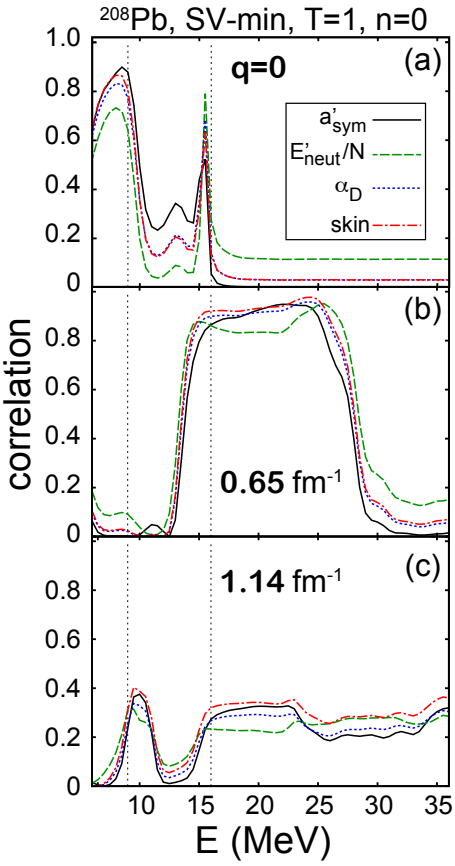

FIG. 9. (Color online) Correlation between the $T = 1$ accumulated E1 strength in ^{208}Pb and selected isovector indicators $(a'_{\rm sym}, E_{\rm neut}/N, \alpha_{\rm D}, r_{\rm skin})$ in SV-min as a function of E for $q = 0$ (a); $q = 0.65\,{\rm fm}^{-1}$ (b); and $q = 1.14\,{\rm fm}^{-1}$ (c).

Fig. 10 illustrates the information content of the accumulated inverse-energy-weighted E1 strength $A^F_{-1}(E)$ with respect to the four isovector observables discussed in the context of Fig. 9. Again, we see that the correlations are similar for all four observables and the $T = 1$ accumulated strength at $q = 0$ nicely correlates with isovector indicators. At $q = 0.65\,{\rm fm}^{-1}$, however, this correlation is weaker; they maximize around $E = 23\,{\rm MeV}$. The accumulated inverse-energy-weighted isoscalar strength does not seem to correlate well with isovector observables.

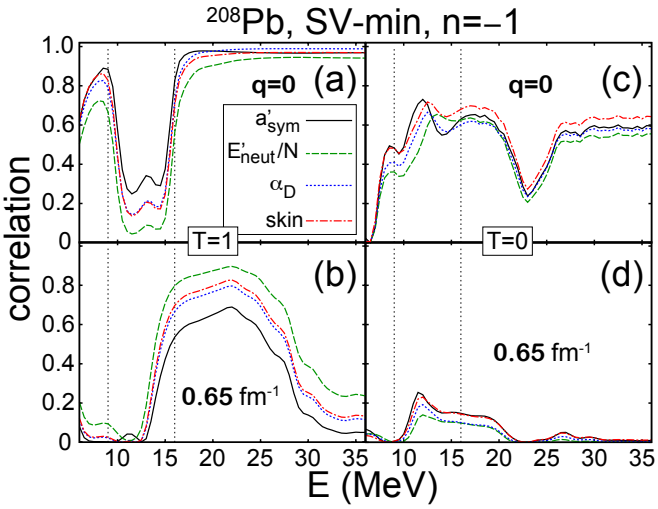

FIG. 10. (Color online) Correlation between the $T = 1$ (left) and $T = 0$ (right) accumulated inverse-energy-weighted E1 strength A^F_{-1} in ^{208}Pb and selected isovector indicators $(a'_{\rm sym}, E_{\rm neut}/N, \alpha_{\rm D}, r_{\rm skin})$ in SV-min as a function of E for $q = 0$ (top) and $q = 0.65\,{\rm fm}^{-1}$ (bottom).

VII. A QUICK GLANCE AT ^{132}Sn

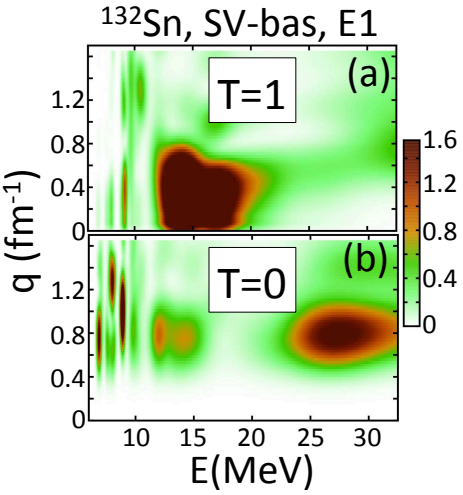

FIG. 11. (Color online) Similar as in Fig. 2, panels (c) and (d), except for ^{132}Sn.

It is interesting to check whether the findings obtained for ^{208}Pb are specific to this nucleus or whether they are of a more general nature. To this end, we inspect the case of a neutron-rich, doubly-magic nucleus ^{132}Sn. Figure 11 shows its $T = 1$ and $T = 0$ E1 strength predicted with SV-bas. The overall pattern, with GDR transitions in the isovector channel and the dominant dipole compressional mode in the isoscalar channel, closely resembles that shown in Fig 2 for ^{208}Pb. In particular, the low-energy modes are isoscalar at low-q values and isoscalar at higher momentum transfer.

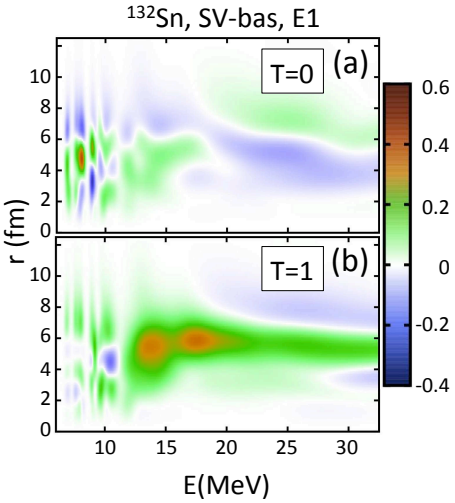

FIG. 12. (Color online) Similar as in Fig. 4, except for ^{132}Sn.

Figure 12 shows the transition densities for ^{132}Sn. Again, the pattern is extremely similar to the case of ^{208}Pb. Finally Fig. 13 shows the correlations of the four basic NMP with accumulated isovector dipole strength. It is, again, similar to the analogous Fig. 7(a) for ^{208}Pb. We also carried out calculations for other neutron-rich

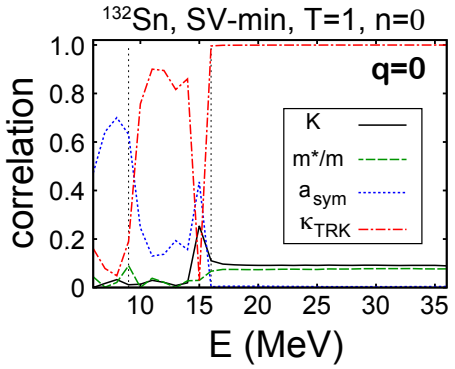

FIG. 13. (Color online) Similar as in Fig. 7(a), except for ^{132}Sn.

nuclei, such as ^{140}Sn, and our conclusion is that the case of ^{208}Pb is representative to other spherical closed-shell heavy systems.

VIII. CONCLUSIONS

To clarify the ambiguous theoretical situation with regard to the interpretation of the low-energy electric dipole strength, we study its information content with respect to isovector and isoscalar indicators characterizing bulk nuclear matter and finite nuclei. As a theoretical tool, we use self-consistent nuclear density functional theory augmented by the random phase approximation. The inter-observable correlations are computed by means of covariance analysis. We use well-calibrated Skyrme energy density functionals that allow for systematic variations of isoscalar and isovector parameters characterizing nuclear matter properties. (The extension of the correlation analysis to other models, including relativistic EDF, will be carried out in a forthcoming study [52].) To avoid ambiguities due to strong shell effects and pairing, our investigations have been limited to the doubly-magic heavy nuclei ^{208}Pb and on ^{132}Sn, and the results were very close in both cases. To separate various electric dipole modes, we study the E1 strength as a function of excitation energy E and momentum transfer q. By going to the q-dimension, we are able to resolve excitation modes that are close in energy, and can nicely separate low-energy excitations from the $T = 1$ and $T = 0$ giant resonances.

Our study fully confirms the main conclusion of our previous work [26]. Namely, the low-energy dipole excitations cannot be interpreted in terms of a collective pygmy dipole resonance mode associated with the motion of skin neutrons. The detailed inspection of transition form factor and density shows a pattern of rapidly varying particle-hole excitations. Moreover, it seems that a large fraction of the low lying states are isovector "shadows" of the underlying low-energy part of the isoscalar compressional mode.

At the level of more global observables, we have studied the E1 strength integrated up to a given cutoff energy. As a first indicator of correlations, we have plotted in Fig. 5 the changes of the low-energy strength with systematically varied nuclear matter properties. This has led to a complex picture where every NMP has some influence on the low energy strength. To assess correlations in a meaningful way, we went beyond the simple inspection of trends and employed the standard tools of statistical analysis. While the local E1 strength at low energies shows some correlations with isovector indicators such as symmetry energy, the magnitude of those correlations varies rapidly around the lower end of the GDR region. This strong dependence on the cutoff energy indicates that a pygmy strength cannot be unambiguously defined; hence, its usefulness might be limited.

Of particular importance are the fully integrated strength; the much celebrated sum rules. The $T = 1$ sum rules, such as the dipole polarizability $\alpha_{\rm D}$ (the inverse energy weighted sum rule), the sum rule enhancement factor κ (strongly correlated with the energy weighted sum rule), and the total accumulated E1 strength are all excellent probes of nuclear isovector properties. At the isoscalar side, we found a relatively strong correlation between nuclear incompressibility and the accumulated isoscalar dipole strength for $q = 0.65\,\mathrm{fm}^{-1}$ (at $E = 9\,\mathrm{MeV}$ and above $20\,\mathrm{MeV}$). In general, experimental studies at $q > 0$ in the isovector and isoscalar channel could provide an excellent window for a better characterization of E1 strength and relating it to fundamental nuclear properties.

ACKNOWLEDGMENTS

This work was initiated during the Workshop on *The Nuclear Dipole Polarizability and its Impact on Nuclear Structure and Astrophysics*, held at ECT* in Trento, June 18-22, 2012. This work was supported by BMBF under contract no. 06 ER 142D and by the Office of Nuclear Physics, U.S. Department of Energy under Contract No. DE-FG02-96ER40963.

[1] A. Bohr and B. Mottelson, *Nuclear Structure, vol. II* (W A. Benjamin, Reading, 1975).
[2] P. Ring and P. Schuck, *The Nuclear Many-Body Problem* (Springer, 2000).
[3] M. N. Harakeh and A. van der Woude, *Giant Resonances: Fundamental High-Frequency Modes of Nuclear Excitation* (Oxford University Press, 2001).
[4] E. Lipparini and S. Stringari, Phys. Lett. B **112**, 421 (1982).
[5] E. Lipparini and S. Stringari, Phys. Rep. **175**, 103 (1989).
[6] P.-G. Reinhard, Nucl. Phys. A **649**, 305c (1999).
[7] W. Satuła, R. A. Wyss, and M. Rafalski, Phys. Rev. C **74**, 011301 (2006).
[8] N. Paar, D. Vretenar, E. Khan, and G. Colò, Rep. Prog. Phys. **70**, 691 (2007).
[9] L. Trippa, G. Colò, and E. Vigezzi, Phys. Rev. C **77**, 061304 (2008).
[10] S. Goriely, Phys. Lett. B **436**, 1 (1998); S. Goriely, E. Khan, and M. Samyn, Nucl. Phys. A **739**, 331 (2004); I. Daoutidis and S. Goriely, Phys. Rev. C **86**, 034328 (2012).
[11] M. Erhard *et al.*, Phys. Rev. C **81**, 034319 (2010); M. Beard, S. Frauendorf, B. Kämpfer, R. Schwengner, and M. Wiescher, *ibid.* **85**, 065808 (2012).
[12] N. Ryezayeva *et al.*, Phys. Rev. Lett. **89**, 272502 (2002).
[13] P. Adrich *et al.* (LAND-FRS Collaboration), Phys. Rev. Lett. **95**, 132501 (2005).
[14] A. Zilges, S. Volz, M. Babilon, T. Hartmann, P. Mohr, and K. Vogt, Phys. Lett. B **542**, 43 (2002); T. Hartmann, M. Babilon, S. Kamerdzhiev, E. Litvinova, D. Savran, S. Volz, and A. Zilges, Phys. Rev. Lett. **93**, 192501 (2004); D. Savran, M. Babilon, A. M. van den Berg, M. N. Harakeh, J. Hasper, A. Matic, H. J. Wörtche, and A. Zilges, *ibid.* **97**, 172502 (2006); D. Savran, M. Fritzsche, J. Hasper, K. Lindenberg, S. Müller, V. Y. Ponomarev, K. Sonnabend, and A. Zilges, *ibid.* **100**, 232501 (2008); J. Endres *et al.*, *ibid.* **105**, 212503 (2010); D. Savran *et al.*, Phys. Rev. C **84**, 024326 (2011); J. Isaak *et al.*, *ibid.* **83**, 034304 (2011); J. Endres *et al.*, *ibid.* **85**, 064331 (2012).
[15] R. Schwengner *et al.*, Phys. Rev. C **78**, 064314 (2008); R. Massarczyk *et al.*, *ibid.* **86**, 014319 (2012).
[16] A. Klimkiewicz *et al.* (LAND Collaboration), Phys. Rev. C **76**, 051603 (2007).
[17] A. P. Tonchev, S. L. Hammond, J. H. Kelley, E. Kwan, H. Lenske, G. Rusev, W. Tornow, and N. Tsoneva, Phys. Rev. Lett. **104**, 072501 (2010).
[18] A. Carbone, G. Colò, A. Bracco, L.-G. Cao, P. F. Bortignon, F. Camera, and O. Wieland, Phys. Rev. C **81**, 041301 (2010); O. Wieland *et al.*, Phys. Rev. Lett. **102**, 092502 (2009).
[19] A. Tamii *et al.*, Phys. Rev. Lett. **107**, 062502 (2011).
[20] J. Brzosko, E. Gierlik, A. Soltan, and Z. Wilhelmi, Can. J. Phys. **47**, 2849 (1968).
[21] A. Lane, Ann. Phys. (NY) **63**, 171 (1971).
[22] J. Piekarewicz, Phys. Rev. C **73**, 044325 (2006).
[23] N. Tsoneva and H. Lenske, Phys. Rev. C **77**, 024321 (2008); N. Tsoneva, H. Lenske, and C. Stoyanov, Phys. Lett. B **586**, 213 (2004).
[24] J. Piekarewicz, Phys. Rev. C **83**, 034319 (2011).
[25] V. Baran, B. Frecus, M. Colonna, and M. Di Toro, Phys. Rev. C **85**, 051601 (2012).
[26] P.-G. Reinhard and W. Nazarewicz, Phys. Rev. C **81**, 051303 (2010).
[27] D. Gambacurta, M. Grasso, and F. Catara, Phys. Rev. C **84**, 034301 (2011).
[28] I. Daoutidis and S. Goriely, Phys. Rev. C **84**, 027301 (2011).
[29] T. Inakura, T. Nakatsukasa, and K. Yabana, Phys. Rev. C **84**, 021302 (2011).
[30] X. Roca-Maza, G. Pozzi, M. Brenna, K. Mizuyama, and G. Colò, Phys. Rev. C **85**, 024601 (2012).
[31] E. Yüksel, E. Khan, and K. Bozkurt, Nucl. Phys. A **877**, 35 (2012).
[32] A. Repko, P.-G. Reinhard, V. Nesterenko, and J. Kvasil, (2012), arXiv:1212.2088.
[33] J. Piekarewicz, B. K. Agrawal, G. Colò, W. Nazarewicz, N. Paar, P.-G. Reinhard, X. Roca-Maza, and D. Vretenar, Phys. Rev. C **85**, 041302 (2012).
[34] D. Vretenar, Y. F. Niu, N. Paar, and J. Meng, Phys. Rev. C **85**, 044317 (2012).
[35] M. Bender, P.-H. Heenen, and P.-G. Reinhard, Rev. Mod. Phys. **75**, 121 (2003).
[36] J. Erler, P. Klüpfel, and P.-G. Reinhard, J. Phys. G **38**, 033101 (2011).
[37] J. W. Negele and D. Vautherin, Phys. Rev. C **5**, 1472 (1972).
[38] B. G. Carlsson and J. Dobaczewski, Phys. Rev. Lett. **105**, 122501 (2010).
[39] P. Klüpfel, P.-G. Reinhard, T. J. Bürvenich, and J. A. Maruhn, Phys. Rev. C **79**, 034310 (2009).
[40] M. Kortelainen, J. McDonnell, W. Nazarewicz, P.-G. Reinhard, J. Sarich, N. Schunck, M. V. Stoitsov, and S. M. Wild, Phys. Rev. C **85**, 024304 (2012).
[41] M. Kortelainen, T. Lesinski, J. Moré, W. Nazarewicz, J. Sarich, N. Schunck, M. V. Stoitsov, and S. Wild, Phys. Rev. C **82**, 024313 (2010).
[42] P. Klüpfel, J. Erler, P.-G. Reinhard, and J. A. Maruhn, Eur. Phys. J A **37**, 343 (2008).
[43] F. J. Fattoyev and J. Piekarewicz, Phys. Rev. C **84**, 064302 (2011).
[44] P.-G. Reinhard and Y. Gambhir, Ann. Phys. (Leipzig) **504**, 598 (1992).
[45] P.-G. Reinhard, Ann. Phys. (Leipzig) **504**, 632 (1992).
[46] N. Van Giai and H. Sagawa, Nucl. Phys. A **371**, 1 (1981).
[47] M. N. Harakeh and A. E. L. Dieperink, Phys. Rev. C **23**, 2329 (1981).
[48] I. Hamamoto, H. Sagawa, and X. Z. Zhang, Phys. Rev.

C **57**, R1064 (1998).
[49] V. M. Kolomietz and S. Shlomo, Phys. Rev. C **61**, 064302 (2000).
[50] J. Kvasil, V. O. Nesterenko, W. Kleinig, P.-G. Reinhard, and P. Vesely, Phys. Rev. C **84**, 034303 (2011).
[51] P. Papakonstantinou, V. Y. Ponomarev, R. Roth, and J. Wambach, Eur. Phys. J. A **47**, 14 (2011); P. Papakonstantinou, H. Hergert, V. Y. Ponomarev, and R. Roth, Phys. Lett. B **709**, 270 (2012).
[52] N. Paar *et al.*, (2012), in preparation.